

# Implications of Einstein-Maxwell dilaton-axion gravity from the black hole continuum spectrum

Indrani Banerjee\*, Bhaswati Mandal† and Soumitra SenGupta‡

School of Physical Sciences, Indian Association for the Cultivation of Science, 2A & 2B Raja S. C. Mullick Road, Kolkata-700032, India

## Abstract

String inspired models can serve as potential candidates to replace general relativity (GR) in the high energy/high curvature regime where quantum gravity is expected to play a vital role. Such models not only subsume the ultraviolet nature of gravity but also exhibit promising prospects in resolving issues like dark matter and dark energy, which cannot be adequately addressed within the framework of GR. The Einstein-Maxwell dilaton-axion (EMDA) theory, which is central to this work is one such string inspired model arising in the low energy effective action of the heterotic string theory with interesting implications in inflationary cosmology and in the late time acceleration of the universe. It is therefore important to survey the role of such a theory in explaining astrophysical observations, e.g. the continuum spectrum of black holes which are expected to hold a wealth of information regarding the background metric. The Kerr-Sen spacetime corresponds to the exact, stationary and axi-symmetric black hole solution in EMDA gravity, possessing dilatonic charge and angular momentum originating from the axionic field. In this work, we compute the theoretical spectrum from the accretion disk around quasars in the Kerr-Sen background assuming the thin accretion disk model due to Novikov & Thorne. This is then used to evaluate the theoretical estimates of optical luminosity for a sample of eighty Palomar-Green quasars which are subsequently compared with the available observations. Our analysis based on error estimators like the  $\chi^2$ , the Nash-Sutcliffe efficiency, the index of agreement etc., indicates that black holes carrying non-existent or weak dilaton charges (viz,  $0 \lesssim r_2 \lesssim 0.1$ ) are observationally more favored. The spins associated with the quasars are also estimated. Interestingly, a similar conclusion has been independently achieved by studying the observed jet power and the radiative efficiencies of microquasars. The implications are discussed.

## 1 Introduction

The remarkable agreement of general relativity (GR) with a host of experimental tests [1–4] makes it the most successful theory of gravity, till date. With the advent of advanced ground-based and space-based missions, the predictions of GR, e.g. presence of black holes and gravitational waves [5–9], have received ever-increasing observational confirmations. Yet, the quest for a more complete theory of gravity continues, as GR is marred with the black hole and big-bang singularities [10–12] and the quantum nature of gravity continues to be elusive [13–15]. On the observational front, general relativity falls short in resolving the

---

\*tpib@iacs.res.in

†tpbm3@iacs.res.in

‡tpssg@iacs.res.in

nature of dark matter and dark energy [16–18], often invoked to explain the galactic rotation curves and the accelerated expansion of the universe, respectively.

This has given birth to a wide variety of alternative gravity models e.g. higher curvature gravity [19–25], extra-dimensional models [26–29] and the scalar-tensor/scalar-vector-tensor theories of gravity [30–33] which can potentially fulfill the deficiencies in GR, yielding GR in the low energy limit. Among the various alternatives to GR, string theory provides an interesting theoretical framework for quantum gravity and force unification. It is often said that it is difficult to detect any signature of string theory in low energy regime. In this context it is important to note that string theory in itself is not a model but provides a framework for building string inspired 4D models which can be confronted with the available observations [34].

This raises the question whether we can discover some footprints of a stringy model in low energy observations. With this aim in mind, in this work we explore the observational signatures of the Einstein-Maxwell dilaton-axion (EMDA) gravity which arises in the low energy effective action of superstring theories [35] when the ten dimensional heterotic string theory is compactified on a six dimensional torus  $T^6$ . Such a scenario consists of  $N = 4$ ,  $d = 4$  supergravity coupled to  $N = 4$  super Yang-Mills theory and can be appropriately truncated to a pure supergravity theory exhibiting  $S$  and  $T$  dualities. The bosonic sector of this  $N = 4$ ,  $d = 4$  supergravity coupled to the  $U(1)$  gauge field is known as the Einstein-Maxwell dilaton-axion (EMDA) gravity [36] which provides a simple framework to study classical solutions. Such a theory comprises of the scalar field dilaton and the pseudo scalar axion coupled to the metric and the Maxwell field. The dilaton and the axion fields are inherited from string compactifications and have interesting implications in the late time acceleration of the universe and inflationary cosmology [37, 38]. It is therefore worthwhile to explore the role of such a theory in astrophysical observations. This has been explored extensively in the past [39–43] in the context of null geodesics, strong gravitational lensing and black hole shadow.

Since deviation from Einstein gravity is expected in the high curvature domain, the near horizon regime of black holes seem to be the ideal astrophysical laboratory to test these models against observations. In particular the continuum spectrum emitted from the accretion disk around black holes bears the imprints of the background spacetime and hence can be used as a promising probe to test the nature of strong gravity. This requires one to look for black hole solutions of these string inspired low-energy effective theories. Fortunately, there exists various classes of black hole solutions bearing non-trivial charges associated with the dilaton and the anti-symmetric tensor gauge fields [44–47]. The stationary and axi-symmetric black hole solution in EMDA gravity corresponds to the charged, rotating Kerr-Sen metric [35] where the electric charge stems from the axion-photon coupling and not the in-falling charged particles. Also, the axionic field renders angular momentum to such black holes. Testing the impact of such a background on the observed spectrum is important since this provides a testbed for string theory.

In this work we compute the continuum spectrum from the accretion disk assuming the spacetime around the black holes to be governed by the Kerr-Sen metric. The presence of dilatonic and axionic charges modify the continuum spectrum from the Kerr scenario. The theoretical spectrum thus computed is compared with the optical data of eighty Palomar Green quasars which allows us to discern the observationally favored magnitude of the dilaton parameter and also estimate the spins of the quasars. We compute several error estimators, e.g. chi-squared, Nash-Sutcliffe efficiency and index of agreement etc. to arrive at our conclusions.

The paper is organised as follows: In Section 2 we describe the Einstein-Maxwell dilaton-axion (EMDA) theory and the Kerr-Sen solution. Section 3 is dedicated to computing the theoretical spectrum from the accretion disk in the Kerr-Sen background. The theoretical spectrum is subsequently compared with the optical observations of eighty Palomar Green quasars and the error estimators are computed in

[Section 4](#). Finally we conclude with a summary of our findings with some scope for future work in [Section 5](#).

Notations and Conventions: Throughout this paper, we use  $(-,+,+,+)$  as the metric convention and will work with geometrized units taking  $G = c = 1$ .

## 2 Einstein-Maxwell dilaton-axion gravity: A brief overview

The Einstein-Maxwell dilaton-axion (EMDA) gravity [35,36] is obtained when the ten dimensional heterotic string theory is compactified on a six dimensional torus  $T^6$ . The action  $\mathcal{S}$  associated with EMDA gravity comprises of couplings between the metric  $g_{\mu\nu}$ , the  $U(1)$  gauge field  $A_\mu$ , the dilaton field  $\chi$  and the third rank anti-symmetric tensor field  $\mathcal{H}_{\mu\nu\alpha}$  such that,

$$\mathcal{S} = \frac{1}{16\pi} \int \sqrt{-g} d^4x \left[ \mathcal{R} - 2\partial_\nu \chi \partial^\nu \chi - \frac{1}{3} \mathcal{H}_{\rho\sigma\delta} \mathcal{H}^{\rho\sigma\delta} + e^{-2\chi} \mathcal{F}_{\rho\sigma} \mathcal{F}^{\rho\sigma} \right] \quad (1)$$

where,  $g$  is the determinant and  $\mathcal{R}$  the Ricci scalar with respect to the 4-dimensional metric  $g_{\mu\nu}$ . In [Eq. \(1\)](#),  $\mathcal{F}_{\mu\nu}$  represents the second rank antisymmetric Maxwell field strength tensor such that  $\mathcal{F}_{\mu\nu} = \nabla_\mu A_\nu - \nabla_\nu A_\mu$  while the dilaton field is denoted by  $\chi$ . The third rank antisymmetric tensor field  $\mathcal{H}_{\rho\sigma\delta}$  in the above action can be expressed in the form,

$$\mathcal{H}_{\rho\sigma\delta} = \nabla_\rho B_{\sigma\delta} + \nabla_\sigma B_{\delta\rho} + \nabla_\delta B_{\rho\sigma} - (A_\rho B_{\sigma\delta} + A_\sigma B_{\delta\rho} + A_\delta B_{\rho\sigma}) \quad (2)$$

where the second rank anti-symmetric tensor gauge field  $B_{\mu\nu}$  in [Eq. \(2\)](#) is known as the Kalb-Ramond field and its cyclic permutation with  $A_\mu$  represents the Chern-Simons term.

In four dimensions  $\mathcal{H}_{\mu\nu\alpha}$  is associated with the pseudo-scalar axion field  $\xi$ , such that,

$$\mathcal{H}_{\rho\sigma\delta} = \frac{1}{2} e^{4\chi} \epsilon_{\rho\sigma\delta\gamma} \partial^\gamma \xi \quad (3)$$

When expressed in terms of the axion field, [Eq. \(1\)](#) assumes the form,

$$\mathcal{S} = \frac{1}{16\pi} \int \sqrt{-g} d^4x \left[ \mathcal{R} - 2\partial_\nu \chi \partial^\nu \chi - \frac{1}{2} e^{4\chi} \partial_\nu \xi \partial^\nu \xi + e^{-2\chi} \mathcal{F}_{\rho\sigma} \mathcal{F}^{\rho\sigma} + \xi \mathcal{F}_{\rho\sigma} \tilde{\mathcal{F}}^{\rho\sigma} \right] \quad (4)$$

By varying the action with respect to the dilaton, axion and the Maxwell fields we obtain their corresponding equations of motion. The equation of motion associated with the dilaton field is given by,

$$\nabla_\mu \nabla^\mu \chi - \frac{1}{2} e^{4\chi} \nabla_\mu \xi \nabla^\mu \xi + \frac{1}{2} e^{-2\chi} \mathcal{F}^2 = 0, \quad (5)$$

while that of the axion is,

$$\nabla_\mu \nabla^\mu \xi + 4\nabla_\nu \xi \nabla^\nu \chi - e^{-4\chi} \mathcal{F}_{\rho\sigma} \tilde{\mathcal{F}}^{\rho\sigma} = 0 \quad (6)$$

The Maxwell's equations coupled to the dilaton and the axion fields are given by,

$$\nabla_\mu (e^{-2\chi} \mathcal{F}^{\mu\nu} + \xi \tilde{\mathcal{F}}^{\mu\nu}) = 0, \quad (7)$$

$$\nabla_\mu (\tilde{\mathcal{F}}^{\mu\nu}) = 0 \quad (8)$$

The solution of the axion, dilaton and the  $U(1)$  gauge fields are respectively given by [35, 36, 48],

$$\xi = \frac{q^2}{\mathcal{M}} \frac{a \cos \theta}{r^2 + a^2 \cos^2 \theta} \quad (9)$$

$$e^{2\chi} = \frac{r^2 + a^2 \cos^2 \theta}{r(r + r_2) + a^2 \cos^2 \theta} \quad (10)$$

$$A = \frac{qr}{\tilde{\Sigma}} \left( -dt + a \sin^2 \theta d\phi \right) \quad (11)$$

From above the non-zero components of  $H_{\mu\nu\alpha}$  can also be evaluated [48].

The gravitational field equations are obtained when the action is varied with respect to  $g_{\mu\nu}$  which yields the Einstein's equations,

$$\mathcal{G}_{\mu\nu} = \mathcal{T}_{\mu\nu}(\mathcal{F}, \chi, \xi) \quad (12)$$

where,  $\mathcal{G}_{\mu\nu}$  is the Einstein tensor and the energy-momentum tensor  $\mathcal{T}_{\mu\nu}$  on the right hand side of Eq. (12) is given by,

$$\mathcal{T}_{\mu\nu}(\mathcal{F}, \chi, \xi) = e^{2\chi}(4\mathcal{F}_{\mu\rho}\mathcal{F}_\nu^\rho - g_{\mu\nu}\mathcal{F}^2) - g_{\mu\nu}(2\partial_\gamma\chi\partial^\gamma\chi + \frac{1}{2}e^{4\chi}\partial_\gamma\xi\partial^\gamma\xi) + \partial_\mu\chi\partial_\nu\chi + e^{4\chi}\partial_\mu\xi\partial_\nu\xi \quad (13)$$

The stationary and axisymmetric solution of the Einstein's equations corresponds to the Kerr-Sen metric [35] which when expressed in Boyer-Lindquist coordinates assumes the form [49–51],

$$ds^2 = -\left(1 - \frac{2\mathcal{M}r}{\tilde{\Sigma}}\right) dt^2 + \frac{\tilde{\Sigma}}{\Delta}(dr^2 + \Delta d\theta^2) - \frac{4a\mathcal{M}r}{\tilde{\Sigma}} \sin^2 \theta dt d\phi + \sin^2 \theta d\phi^2 \left[ r(r + r_2) + a^2 + \frac{2\mathcal{M}ra^2 \sin^2 \theta}{\tilde{\Sigma}} \right] \quad (14)$$

where,

$$\tilde{\Sigma} = r(r + r_2) + a^2 \cos^2 \theta \quad (14a)$$

$$\Delta = r(r + r_2) - 2\mathcal{M}r + a^2 \quad (14b)$$

In Eq. (14),  $\mathcal{M}$  is the mass,  $r_2 = \frac{q^2}{\mathcal{M}}e^{2\chi_0}$  is the dilaton parameter and  $a$  is the angular momentum associated with the black hole. The dilaton parameter bears the imprints of the asymptotic value of the dilatonic field  $\chi_0$  and the electric charge  $q$  of the black hole. This charge essentially originates from the axion-photon coupling and not the in-falling charged particles since without the electric charge the field strengths corresponding to both the axion and the dilaton vanish (Eq. (9) and Eq. (10)). In such a scenario, Eq. (14) reduces to the Kerr metric. We further note that in Eq. (14) the spin of the black hole originates from the axion field since a non-rotating black hole ( $a = 0$ ) leads to a vanishing axionic field strength (Eq. (9)). When the rotation parameter in Eq. (14) vanishes, the resultant spherically symmetric spacetime represents a pure dilaton black hole labelled by its mass, electric charge and the asymptotic value of the dilaton field [45, 52].

The event horizon  $r_H$  of the Kerr-Sen spacetime is obtained by solving for  $\Delta = 0$  such that,

$$r_H = \mathcal{M} - \frac{r_2}{2} + \sqrt{\left(\mathcal{M} - \frac{r_2}{2}\right)^2 - a^2} \quad (15)$$

From Eq. (15) and the fact that  $r_2$  depends on the square of the electric charge, it can be shown that  $0 \leq \frac{r_2}{\mathcal{M}} \leq 2$  leads to real, positive event horizons and hence black hole solutions. In this work we will be interested in this regime of  $r_2$ .

In the next section we will discuss accretion in the Kerr-Sen background and explicitly demonstrate the dependence of the luminosity from the accretion disk on the background spacetime.

### 3 Spectrum from the accretion disk around black holes in the Kerr-Sen spacetime

The continuum spectrum emitted from the accretion disk surrounding the black holes is sensitive to the background metric and hence provides an interesting observational avenue to explore the signatures of the Kerr-Sen spacetime. In this section, we will compute the continuum spectrum from the accretion disk in a general stationary, axi-symmetric background and subsequently specialize to the Kerr-Sen metric. This in turn will enable us to probe the observable effects of EMDA gravity which can be used to distinguish it from the general relativistic scenario.

The continuum spectrum depends not only on the background metric but also on the properties of the accretion flow. In this work we will derive the continuum spectrum based on the Novikov-Thorne model which adopts the ‘thin-disk approximation’ [53, 54]. In such a scenario, the accretion takes place along the equatorial plane ( $\theta = \pi/2$  plane) such that the resultant accretion disk is geometrically thin with  $\frac{h(r)}{r} \ll 1$ ,  $h(r)$  being the height of the disk at a radial distance  $r$ . The accreting particles are assumed to maintain *nearly circular* geodesics such that the azimuthal velocity  $u_\phi$  much exceeds the radial and the vertical velocity  $u_r$  and  $u_z$  respectively, i.e.  $u_z \ll u_r \ll u_\phi$ . The presence of viscous stresses imparts minimal radial velocity to the accreting fluid which facilitates gradual inspiral and fall of matter into the black hole. Since the vertical velocity is negligible, a thin accretion disk harbors *no outflows*.

The energy-momentum tensor associated with the accreting fluid can be expressed as,

$$T_\beta^\alpha = \rho_0 (1 + \Pi) u^\alpha u_\beta + t_\beta^\alpha + u^\alpha q_\beta + q^\alpha u_\beta , \quad (16)$$

where  $\rho_0$  is the proper density and  $u^\alpha$  is the four velocity of the accreting particles such that the term  $\rho_0 u^\mu u^\nu$  represent the contribution to the energy-momentum tensor due to the geodesic flow. The specific internal energy of the system is denoted by  $\Pi$  and the associated term denotes the contribution to the energy density due to dissipation. In Eq. (16),  $t^{\alpha\beta}$  and  $q^\alpha$  respectively denote the stress-tensor and the energy flux relative to the local inertial frame and consequently  $t_{\alpha\beta} u^\alpha = 0 = q_\alpha u^\alpha$ . Motion of the particles along the geodesics ensures that the gravitational pull of the central black hole dominates the forces due to radial pressure gradients and hence the specific internal energy of the accreting fluid can be ignored compared to its rest energy. Therefore, the special relativistic corrections to the local thermodynamic, hydrodynamic and radiative properties of the fluid can be safely neglected compared to the general relativistic effects of the black hole [53, 54]. The loss of gravitational potential energy due to infall of matter towards the black hole generates electromagnetic radiation which interacts efficiently with the accreting fluid before being radiated out of the system. Since the specific internal energy  $\Pi \ll 1$ , the accreting fluid retains no heat and the only the z-component of the energy flux vector  $q^\alpha$  has a non-zero contribution to the energy-momentum tensor.

In order to compute the flux and hence the luminosity from the accretion disk we assume that the black hole undergoes steady state accretion at a rate  $\dot{M}$  and the accreting fluid obeys conservation of

mass, energy and angular momentum. The conservation of mass assumes the form,

$$\dot{M} = -2\pi\sqrt{-g}u^r\Sigma \quad (17)$$

where  $\Sigma$  denotes the average surface density of matter flowing into the black hole and  $g$  corresponds to the determinant of the metric. The conservation of angular momentum and energy are respectively given by,

$$\frac{\partial}{\partial r} \left[ \dot{M}\mathcal{L} - 2\pi\sqrt{-g}W_\phi^r \right] = 4\pi\sqrt{-g}F\mathcal{L} \quad , \quad \text{and} \quad (18)$$

$$\frac{\partial}{\partial r} \left[ \dot{M}\mathcal{E} - 2\pi\sqrt{-g}\Omega W_\phi^r \right] = 4\pi\sqrt{-g}F\mathcal{E} \quad (19)$$

where  $\Omega$ ,  $\mathcal{E}$  and  $\mathcal{L}$  are the angular velocity, the specific energy and the specific angular momentum of the accreting fluid. In a stationary and axi-symmetric spacetime  $\mathcal{E}$  and  $\mathcal{L}$  are conserved and can be expressed in terms of the metric coefficients such that,

$$\mathcal{E} = \frac{-g_{tt} - \Omega g_{t\phi}}{\sqrt{-g_{tt} - 2\Omega g_{t\phi} - \Omega^2 g_{\phi\phi}}} \quad , \quad (20)$$

$$\mathcal{L} = \frac{\Omega g_{\phi\phi} + g_{t\phi}}{\sqrt{-g_{tt} - 2\Omega g_{t\phi} - \Omega^2 g_{\phi\phi}}} \quad . \quad (21)$$

and the angular velocity  $\Omega$  is given by,

$$\Omega = \frac{d\phi}{dt} = \frac{-g_{t\phi,r} \pm \sqrt{\{-g_{t\phi,r}\}^2 - \{g_{\phi\phi,r}\}\{g_{tt,r}\}}}{g_{\phi\phi,r}} \quad (22)$$

Since the motion is along the equatorial plane  $\mathcal{E}$  and  $\mathcal{L}$  are only functions of the radial coordinate and the  $g_{\theta\theta}$  component does not contribute to the conserved quantities.

In Eq. (18) and Eq. (19),  $F$  denotes the flux of radiation generated by the accretion process and is given by,

$$F \equiv \langle q^z(r, h) \rangle = \langle -q^z(r, -h) \rangle \quad (23)$$

while  $W_\phi^r$  is associated with the time and height averaged stress tensor in the local rest frame of the accreting particles, i.e.,

$$W_\beta^\alpha = \int_{-h}^h dz \langle t_\beta^\alpha \rangle \quad (24)$$

By manipulating the conservation laws an analytical expression for the flux  $F$  from the accretion disk can be obtained, such that,

$$F = \frac{\dot{M}}{4\pi\sqrt{-g}}f \quad \text{where} \quad (25)$$

$$f = -\frac{\Omega_{,r}}{(\mathcal{E} - \Omega\mathcal{L})^2} \left[ \mathcal{E}\mathcal{L} - \mathcal{E}_{ms}\mathcal{L}_{ms} - 2 \int_{r_{ms}}^r \mathcal{L}\mathcal{E}_{,r'} dr' \right] \quad (26)$$

While deriving Eq. (25) the viscous stress  $W_\phi^r$  is assumed to vanish at the marginally stable circular orbit  $r_{ms}$ , such that after crossing this radius the azimuthal velocity of the accreting fluid vanishes and radial accretion takes over. The last stable circular orbit  $r_{ms}$ , corresponds to the inflection point of the effective potential in which the accreting particles move. The effective potential  $V_{eff}$  is given by [55],

$$V_{eff}(r) = \frac{\mathcal{E}^2 g_{\phi\phi} + 2\mathcal{E}\mathcal{L}g_{t\phi} + \mathcal{L}^2 g_{tt}}{g_{t\phi}^2 - g_{tt}g_{\phi\phi}} - 1 \quad (27)$$

and  $r_{ms}$  is obtained by solving for  $V_{eff} = \partial_r V_{eff} = \partial_r^2 V_{eff} = 0$ . In Eq. (26)  $\mathcal{E}_{ms}$  and  $\mathcal{L}_{ms}$  denote the energy and angular momentum at the marginally stable circular orbit.

Since the electromagnetic radiation emitted due to loss of gravitational potential energy undergoes repeated collisions with the accreting fluid, a thermal equilibrium between matter and radiation is established. This renders the accretion disk to be geometrically thin and optically thick such that it emits locally as a black body. Therefore, the temperature profile is given by the Stefan-Boltzmann law, i.e.,  $T(r) = (\mathcal{F}(r)/\sigma)^{1/4}$  ( $\sigma$  being the Stefan-Boltzmann constant) and  $\mathcal{F}(r) = F(r)c^6/G^2\mathcal{M}^2$  (where  $F(r)$  is given by Eq. (25) and Eq. (26)). Hence the accretion disk emits a Planck spectrum at every radius with a peak temperature  $T(r)$ . Finally, the luminosity  $L_\nu$  emitted by the disk at an observed frequency  $\nu$  is obtained by integrating the Planck function  $B_\nu(T(r))$  over the disk surface,

$$L_\nu = 8\pi^2 r_g^2 \cos i \int_{x_{ms}}^{x_{out}} \sqrt{g_{rr}} B_\nu(T) x dx; \quad B_\nu(T) = \frac{2h\nu^3/c^2}{\exp\left(\frac{h\nu}{z_g kT}\right) - 1} \quad (28)$$

where,  $x = r/r_g$  is the radial coordinate expressed in units of the gravitational radius  $r_g = GM/c^2$  and “ $i$ ” is the inclination angle between the line of sight and the normal to the disk. In Eq. (28)  $z_g$  is the gravitational redshift factor given by,

$$z_g = \mathcal{E} \frac{\sqrt{-g_{tt} - 2\Omega g_{t\phi} - \Omega^2 g_{\phi\phi}}}{\mathcal{E} - \Omega\mathcal{L}} \quad (29)$$

which is associated with the change in the frequency suffered by the photon while travelling from the emitting material to the observer [56].

We have thus arrived at an analytical expression for the luminosity from the accretion disk given by Eq. (28). We note that it depends on the background metric through the energy, angular momentum, angular velocity and the radius of the marginally stable circular orbit, where in the present work we will consider the metric components corresponding to the Kerr-Sen spacetime given by Eq. (14). Apart from the metric parameters, the spectrum is also sensitive to the mass of the black hole, the accretion rate and the inclination angle of the disk to the line of sight.

Fig. 1 depicts the variation of the theoretically derived luminosity from the accretion disk with the frequency, for two different masses of the supermassive black holes, viz,  $\mathcal{M} = 10^9 M_\odot$  and  $\mathcal{M} = 10^7 M_\odot$ . The accretion rate is assumed to be  $1M_\odot \text{yr}^{-1}$  while the inclination angle is considered to be  $\cos i = 0.8$ . We note that the spectrum from a lower mass black hole peaks at a higher frequency which can be ascribed to the  $T \propto \mathcal{M}^{-1/4}$  dependence of the peak temperature  $T$  for a multi-color black body spectrum with the black hole mass [57]. It is evident from Fig. 1 that the metric parameters  $r_2$  and  $a$  substantially affect the

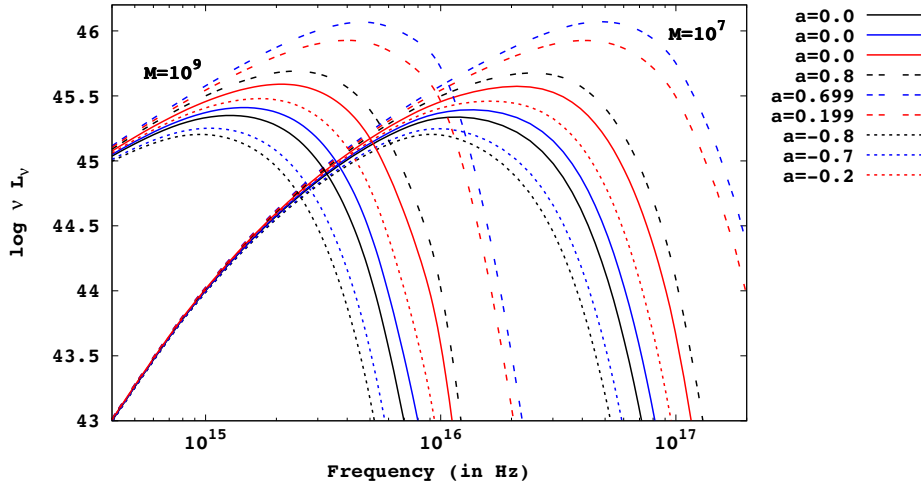


Figure 1: The above figure depicts the variation of the theoretically derived luminosity from the accretion disk with frequency for two different masses of the supermassive black holes, namely,  $M = 10^7 M_\odot$  and  $M = 10^9 M_\odot$ . For both the masses, the black lines represent  $r_2 = 0$ , while the blue and red lines correspond to  $r_2 = 0.6$  and  $r_2 = 1.6$  respectively. For a given  $r_2$ , prograde spins are denoted by dashed lines, non-rotating black holes are denoted by solid lines while their retrograde counterparts are illustrated by the dotted lines. The Schwarzschild scenario is depicted by the solid black line. The accretion rate is assumed to be  $1M_\odot\text{yr}^{-1}$  and the inclination angle is taken to be  $\cos i = 0.8$ . For more discussions see text.

luminosity from the accretion disk, specially at high frequencies. We recall from previous discussion that for the existence of the event horizon, the spin of the black hole should lie in the range:  $-(1 - \frac{r_2}{2}) \leq a \leq (1 - \frac{r_2}{2})$  for a given  $r_2$  (Eq. (15)), where  $a$  and  $r_2$  are expressed in units of  $\mathcal{M}$ , which will be considered throughout the remaining discussion. We study three different dilaton parameters in Fig. 1,  $r_2 = 0$  (black lines),  $r_2 = 0.6$  (blue lines) and  $r_2 = 1.6$  (red lines). For each dilaton parameter we consider non-rotating black holes (solid lines) as well as the prograde (dashed lines) and retrograde (dotted lines) spins in the allowed range. We note that for a given  $r_2$  the disk luminosity associated with prograde black holes is maximum followed by the luminosity corresponding to their non-spinning and the retrograde counterparts. Similarly, for a given spin, accretion disks around dilaton black holes are more luminous compared to the general relativistic scenario.

## 4 Numerical Analysis

In this section we compute the optical luminosity of a sample of Palomar Green (PG) quasars [58, 59] assuming the thin accretion disk model discussed in the last section. The optical luminosity  $L_{opt} \equiv \nu L_\nu$  is evaluated at the wavelength  $4861\text{\AA}$  [59] and compared with the corresponding observed values [59] which in turn allows us to discern the observationally favored magnitude of the dilaton parameter and the black hole spins. These quasars have independent mass measurements based on the method of reverberation mapping [60–63] while the accretion rates of the quasars are reported in [59]. Since quasars are mostly

face-on systems, the inclination angle  $i$  is assumed to lie in the range:  $\cos i \in (0.5, 1)$ . Following [59, 64] we adopt a typical value of  $\cos i \sim 0.8$  in our analysis. This is in agreement with the results of Piotrovich et al. [65] who estimated the inclination angle of some of these quasars using the degree of polarisation of the scattered radiation from the accretion disk.

The bolometric luminosities of these quasars have been estimated [59] based on the observed data in the optical [66], UV [67], far-UV [68], and soft X-rays [69]. The error in bolometric luminosity receives dominant contribution from the far-UV extrapolation since the uncertainty in the UV luminosity supercedes other sources of error (e.g., optical or X-ray variability) [59]. Moreover, the UV part of the spectral energy distribution (SED) is contaminated by components other than the accretion disk since physical mechanisms e.g. advection, a Comptonizing corona, etc. may redistribute the UV flux to the X-ray frequencies [59]. Therefore, although the maximum emission from the accretion disk for quasars generally peaks in the optical/UV part of the spectrum, disentangling the role of the metric from UV observations become difficult due to the aforesaid reasons. This motivates us to dwell in the optical domain and compare the optical observations of quasars with the corresponding theoretical estimates.

The requirement for the quasars to possess a real, positive event horizon imposes the constraint  $0 \leq r_2 \leq 2$  on the dilaton parameter. Also, for a given  $r_2$ , the spin  $a$  of the black hole can assume values between,  $-(1 - \frac{r_2}{2}) \leq a \leq (1 - \frac{r_2}{2})$ . In order to arrive at the most favored dilaton parameter we proceed in the following way:

- We consider a quasar in the sample with known  $\mathcal{M}$  and  $\dot{M}$  and compute the theoretical optical luminosity at  $4861\text{\AA}$  for a given  $r_2$  and all the allowed values of  $a$  for that  $r_2$ . The value of  $a$  that best reproduces the observed luminosity, is considered to be the spin of that quasar for the chosen  $r_2$ .
- We repeat the above procedure for all the quasars in the sub-sample for the aforesaid  $r_2$ . This assigns a specific spin for each of the quasars, for the given  $r_2$ .
- We now vary  $r_2$  in the theoretically allowed range, ( $0 \leq r_2 \leq 2$ ) and repeat the above two procedures. This ensures that for every  $r_2$ , the sample of quasars are associated with a spin that minimizes the error between the theoretical and the observed optical luminosities.

In order to arrive at the magnitude of  $r_2$  favored by optical observations of quasars, we compute several error estimators which we discuss next.

## 4.1 Error estimators

In this section we discuss various error estimators which enable us to find the dilaton parameter  $r_2$  minimizing the error between the theoretical and the observed optical luminosities.

- **Chi-square  $\chi^2$**  : We consider the sample of quasars with observed optical luminosities  $\{\mathcal{O}_k\}$  and errors  $\{\sigma_k\}$ . The theoretical estimates of the optical luminosity corresponds to  $\{\mathcal{T}_k(r_2, \{a_{(i)}\})\}$  for a given  $r_2$  (where  $\{a_{(i)}\}$  denotes the set of best choice of spin parameters associated with the quasars for that  $r_2$ , as discussed above). With this, the chi-square ( $\chi^2$ ) of the distribution can be defined as,

$$\chi^2(r_2, \{a_{(i)}\}) = \sum_k \frac{\{\mathcal{O}_k - \mathcal{T}_k(r_2, \{a_{(i)}\})\}^2}{\sigma_k^2}. \quad (30)$$

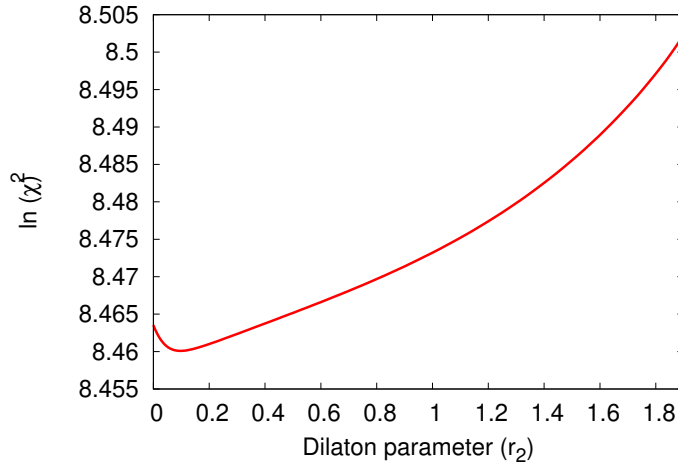


Figure 2: The figure illustrates the variation of  $\chi^2$  with the dilaton parameter  $r_2$  for a sample of eighty quasars.

The errors associated with the optical luminosities are not explicitly reported [59]. However, we have already mentioned that the error in optical luminosity can be ignored compared to the error in bolometric luminosity which receives maximum contribution from the far-UV extrapolation since the uncertainty in the UV luminosity dominates over other sources of error (e.g., optical or X-ray variability) [59]. Therefore, we consider the errors in the bolometric luminosity reported in [59], as the maximum possible error in the estimation of the optical luminosity.

It is important to recall that there are restrictions in the magnitude of  $r_2$  and  $a$  (as discussed in the last section) and one cannot assume arbitrary values of these parameters. Consequently we cannot use reduced chi-square  $\chi_{Red}^2$ , where  $\chi_{Red}^2 = \chi^2/\nu$ , ( $\nu$  being the degrees of freedom) as an error estimator, since the definition of the degrees of freedom becomes ambiguous [70] in such cases. We therefore analyze the error between the theoretical and the observed optical luminosities using  $\chi^2$  as the error estimator.

From the definition of  $\chi^2$  in Eq. (30), it is clear that the magnitude of  $r_2$  which minimizes  $\chi^2$  is most favored by the observations. In Fig. 2 we plot the variation of  $\chi^2$  with the dilaton parameter  $r_2$ . The figure clearly reveals that  $r_2 \sim 0.1$  minimizes the  $\chi^2$  signalling that axion-dilaton black holes with mild dilaton charges are more favored by quasar optical data. The spin of the quasars  $\{a_{(i)}\}$  corresponding to  $r_2 = 0.1$  which can best explain the data are reported in Table 1. At this point it may be worthwhile to mention that in a previous work [55] we compared the theoretical estimates of optical luminosity for braneworld black holes (which can accommodate a negative tidal charge) with the optical data of the same quasar sample. A similar analysis resulted in the conclusion that black holes carrying negative tidal charge (realised in a higher dimensional scenario) are more favored compared to general relativity.

In what follows we consider a few more error estimators in order to verify our conclusion.

- **Nash-Sutcliffe Efficiency:** This particular error estimator denoted by  $E$  [71–73] is associated with

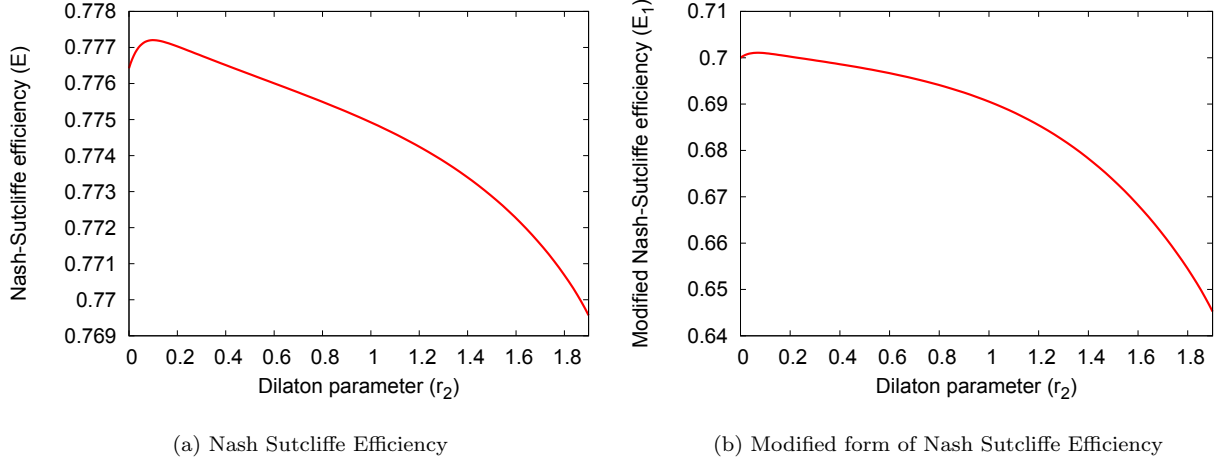


Figure 3: The above figure depicts variation of (a) the Nash-Sutcliffe Efficiency  $E$  and (b) the modified form of the Nash-Sutcliffe Efficiency  $E_1$  with the dilaton parameter  $r_2$ . Both the error estimators maximize when  $0 \lesssim r_2 \lesssim 0.1$ .

the the sum of the squared differences between the observed and the theoretical values normalized by the variance of the observed values. The functional form of the Nash-Sutcliffe Efficiency is given by,

$$E(r_2, \{a_{(i)}\}) = 1 - \frac{\sum_k \{\mathcal{O}_k - \mathcal{T}_k(r_2, \{a_{(i)}\})\}^2}{\sum_k \{\mathcal{O}_k - \mathcal{O}_{av}\}^2} \quad (31)$$

where,  $\mathcal{O}_{av}$  represents the mean value of the observed optical luminosities of the PG quasars.

In contrast to  $\chi^2$ , the dialton parameter which maximizes  $E$  is most favored by observations. Interestingly  $E$  can range from  $-\infty$  to 1. Negative  $E$  indicates that the average of the observed data explains the observation better than the theoretical model. Similarly,  $E \sim 1$  represents the ideal model which predicts the observations with great accuracy [74]. The variation of the Nash-Sutcliffe efficiency with  $r_2$  is illustrated in Fig. 3a. We note that  $E$  maximizes when  $r_2 \sim 0.1$  thereby supporting our earlier conclusion derived from chi-square. The maximum value of Nash-Sutcliffe efficiency  $E_{max} \sim 0.777$ , which is shows that this is a satisfactory model representing the data [74]

- **Modified Nash-Sutcliffe Efficiency  $E_1$  :** In order to overcome the oversensitivity of the Nash-Sutcliffe efficiency to higher values of the optical luminosity, (which arises due to the presence of the square of the error in the numerator) a modified version of the same is proposed [72] which is given by,

$$E_1(r_2, \{a_{(i)}\}) = 1 - \frac{\sum_k |\mathcal{O}_k - \mathcal{T}_k(r_2, \{a_{(i)}\})|}{\sum_k |\mathcal{O}_k - \mathcal{O}_{av}|} \quad (32)$$

This modified estimator exhibits an enhanced sensitivity towards the lower values of the observed optical luminosities. Similar to Nash-Sutcliffe Efficiency, the most favorable  $r_2$  maximizes its modified

version as well. It is observed from the Fig. 3b that this maximization occurs at  $r_2 \sim 0$  which implies that the general relativistic scenario is more favored compared to the EMDA gravity.

- **Index of Agreement and its modified form :** The Nash-Sutcliffe efficiency and its modified form turns out to be insensitive towards the differences between the theoretical and the observed luminosities from the corresponding observed mean [72]. This is overcome by introducing the index of agreement  $d$  [73, 75, 76] where,

$$d(r_2, \{a_{(i)}\}) = 1 - \frac{\sum_k \{\mathcal{O}_k - \mathcal{T}_k(r_2, \{a_{(i)}\})\}^2}{\sum_k \{|\mathcal{O}_k - \mathcal{O}_{av}| + |\mathcal{T}_k(r_2, \{a_{(i)}\}) - \mathcal{O}_{av}|\}^2} \quad (33)$$

and  $\mathcal{O}_{av}$  refers to the average value of the observed luminosities. The denominator, known as the potential error, is related to the maximum value by which each pair of observed and predicted luminosities differ from the average observed luminosity.

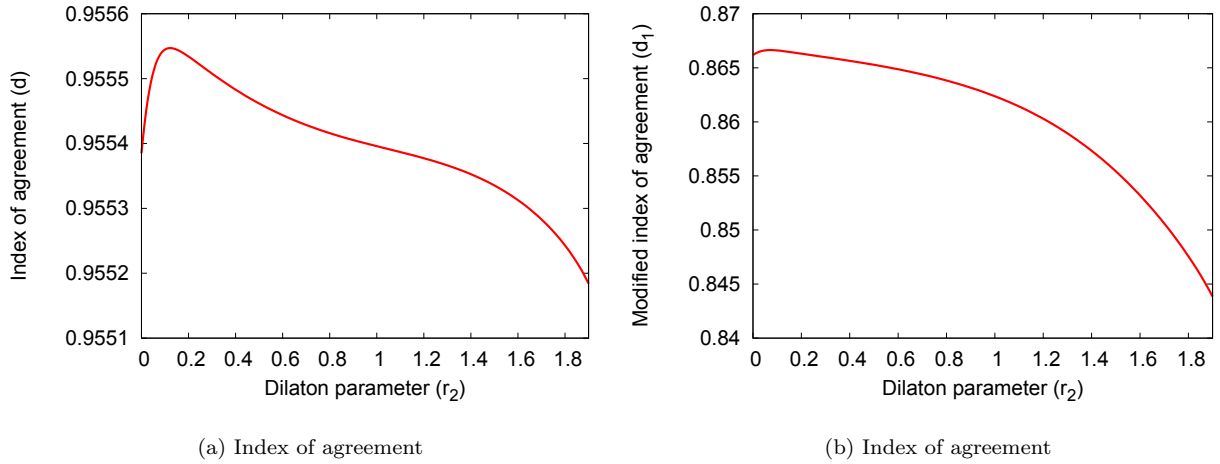


Figure 4: The above figure depicts variation of (a) the index of agreement  $d$  and (b) the modified form of the index of agreement  $d_1$  with the dilaton parameter  $r_2$ . Both the error estimators maximize when  $0 \lesssim r_2 \lesssim 0.1$ . For discussion see text.

Similar to Nash-Sutcliffe Efficiency, the index of agreement is also oversensitive to higher values of the optical luminosity due to the presence of the squared luminosities in the numerator. Therefore, a modified version of the same denoted by  $d_1$  is proposed which assumes the form,

$$d_1(r_2, \{a_{(i)}\}) = 1 - \frac{\sum_k |\mathcal{O}_k - \mathcal{T}_k(r_2, \{a_{(i)}\})|}{\sum_k \{|\mathcal{O}_k - \mathcal{O}_{av}| + |\mathcal{T}_k(r_2, \{a_{(i)}\}) - \mathcal{O}_{av}|\}} \quad (34)$$

It is clear from Eq. (33) and Eq. (34) that the dilaton parameter which maximizes the index of agreement and its modified form best explains the data. Fig. 4a and Fig. 4b respectively illustrates the variation of  $d$  and  $d_1$  with  $r_2$ . We note that  $d$  maximizes when  $r_2 \sim 0.1$  while  $d_1$  attains the maximum at  $r_2 \sim 0$ .

By studying the variation of the error estimators we note that the dilaton parameter which best explains the observations correspond to  $0 \lesssim r_2 \lesssim 0.1$ , indicating that the Kerr scenario or mildly charged dilaton-axion black holes are more favored. In another work [77] we investigated the effect of the Einstein-Maxwell dilaton axion gravity on the power associated with ballistic jets and the radiative efficiencies derived from the continuum spectrum. The theoretical jet power and the radiative efficiencies derived in the Kerr-Sen background were compared with the available observations of microquasars. Such a study reveals that general relativity is more favored compared to the Einstein-Maxwell dilaton-axion scenario, thereby reinforcing our present findings from other independent observations using a different observational sample. It is however important to note that there exists several alternative gravity theories whose black hole solutions resemble the Kerr geometry in general relativity. Therefore, an observational verification of the Kerr solution cannot distinguish these modified gravity models from general relativity [78]. On the other hand, if deviations from general relativity are detected, then it will require revisiting our understanding of gravity in the high curvature domain. Interestingly, a similar analysis with the present quasar sample, when performed with braneworld blackholes (resembling the Kerr-Newman spacetime, although the tidal charge parameter can also accommodate negative values) indicate that quasars with a negative tidal charge (realised in a higher dimensional scenario) are more favored [55, 79]. Since quasars are rotating in nature it is worthwhile to provide an estimate of the spins of the quasars from the above analysis. This is addressed in the next section.

## 4.2 Estimating the spins of the quasars

We have already discussed in the last section that the dilaton parameter which best describes the optical observations of quasars lies in the range  $0 \lesssim r_2 \lesssim 0.1$ . We now discuss the most favored values of the spins of the quasars from the same observations. The procedure for extracting the observationally favored spin parameters of the quasar sample, for a given  $r_2$ , has already been discussed in Section 4. Since the most favored dilaton parameter lies between  $0 - 0.1$ , we report the spins of the quasars for  $r_2 \sim 0.1$  and  $r_2 \sim 0$  in Table 1.

Before presenting the bounds on the spin we note that the theoretically estimated optical luminosity  $L_{opt}$  depends both on the radius of the marginally stable circular orbit  $r_{ms}$  and the outer extension of the accretion disk  $r_{out}$  (Eq. (28)). However, emission from the inner radius has a much greater contribution to the total disk luminosity compared to the outer parts of the disk, since the flux from the accretion disk peaks close to the marginally stable circular orbit  $r_{ms}$ . Therefore, the choice of the outer disk radius  $r_{out}$  is not expected to significantly affect our results. In the present work we have taken  $r_{out} \sim 500 r_g$  [80, 81], however, we have verified that even if the theoretical luminosity  $L_{opt}$  is estimated based on  $r_{out} \sim 1000 r_g$ , our conclusions regarding the most favorable  $r_2$  remain unchanged.

Interestingly, for some of the quasars in our sample, changing  $r_{out}$  does affect the best choice of spins corresponding to a given  $r_2$ . This is because, apart from the metric parameters, the theoretical optical luminosity is sensitive to  $\mathcal{M}$  and  $\dot{M}$  which varies between quasars. For a given  $r_2$  and  $a$ , the ratio  $\dot{M}/\mathcal{M}^2$  determines how sharply peaked the temperature profile  $T(r)$  is near  $r_{ms}$  (see Eq. (25), Eq. (26) and Eq. (28)). In the event,  $T(r)$  is sharply peaked near  $r_{ms}$  the outer disk has negligible contribution to the disk luminosity and the choice of  $r_{out}$  does not play a significant role in such cases. This turns out to be a limitation in our method of estimating the spin since the physical extent of the accretion disk should not modify the angular momentum of the quasars. Therefore we report the spin of only those quasars in Table 1 which remain unaltered by variation of  $r_{out}$ . The most favored values of spin corresponding to  $r_2 \sim 0.1$  and  $r_2 \sim 0$  are presented in Table 1 since the error minimizes for  $0 \lesssim r_2 \lesssim 0.1$ . These are compared with the previously available spin estimates of the quasars, although it is important to note that

Object	log m	log $\dot{m}$	log $L_{\text{obs}}$	log $L_{\text{bol}}$	$a_{r_2=0.1}$	$a_{r_2=0}$
0003 + 199	6.88	-0.06	43.91	45.13 ± 0.35	0.95	0.99
0026 + 129	7.74	0.80	44.99	46.15 ± 0.29	0.95	0.99
0043 + 039	8.98	0.36	45.47	45.98 ± 0.02	-0.3	-0.3
0050 + 124	6.99	0.58	44.41	45.12 ± 0.04	0.95	0.99
0921 + 525	6.87	-0.55	43.56	44.47 ± 0.14	0.95	0.99
0923 + 129	6.82	-0.49	43.58	44.53 ± 0.15	0.95	0.99
0923 + 201	8.84	-0.47	44.81	45.68 ± 0.05	0.3	0.3
1001 + 054	7.47	0.59	44.69	45.36 ± 0.12	0.95	0.99
1011 - 040	6.89	0.17	44.08	45.02 ± 0.23	0.95	0.99
1022 + 519	6.63	-0.36	43.56	45.10 ± 0.39	0.95	0.99
1048 - 090	9.01	0.30	45.45	46.57 ± 0.32	-0.1	-0.1
1049 - 006	8.98	0.34	45.46	46.29 ± 0.15	-0.2	-0.2
1100 + 772	9.13	0.29	45.51	46.61 ± 0.25	0.1	0.1
1103 - 006	9.08	0.21	45.43	46.19 ± 0.10	0.1	0.1
1115 + 407	7.38	0.49	44.58	45.59 ± 0.21	0.95	0.99
1119 + 120	7.04	-0.06	44.01	45.18 ± 0.34	0.95	0.99
1126 - 041	7.31	-0.02	44.19	45.16 ± 0.28	0.95	0.99
1211 + 143	7.64	0.68	44.85	46.41 ± 0.50	0.95	0.99
1226 + 023	9.01	1.18	46.03	47.09 ± 0.24	-0.95	-1.0
1244 + 026	6.15	0.15	43.70	44.74 ± 0.22	0.95	0.99
1259 + 593	8.81	0.99	45.79	47.04 ± 0.29	-0.95	-1.0
1302 - 102	8.76	0.92	45.71	46.51 ± 0.12	-0.95	-1.0
1351 + 236	8.10	-1.14	43.93	44.57 ± 0.12	0.1	0.1
1351 + 640	8.49	-0.38	44.69	45.31 ± 0.05	0.0	0.0
1402 + 261	7.64	0.63	44.82	46.07 ± 0.27	0.95	0.99
1404 + 226	6.52	0.55	44.16	45.21 ± 0.26	0.95	0.99
1416 - 129	8.74	-0.21	44.94	45.82 ± 0.23	0.0	0.0
1425 + 267	9.53	0.07	45.55	46.35 ± 0.20	0.5	0.5
1426 + 015	8.67	-0.49	44.71	45.84 ± 0.24	0.2	0.2
1440 + 356	7.09	0.43	44.37	45.62 ± 0.29	0.95	0.99
1512 + 370	9.20	0.20	45.48	47.11 ± 0.50	0.2	0.2
1519 + 226	7.52	0.18	44.45	45.98 ± 0.41	0.95	0.99
1535 + 547	6.78	-0.01	43.90	44.34 ± 0.02	0.95	0.99
1543 + 489	7.78	1.18	45.27	46.43 ± 0.25	0.95	0.99
1545 + 210	9.10	0.01	45.29	46.14 ± 0.13	0.2	0.2
1552 + 085	7.17	0.56	44.50	45.04 ± 0.01	0.95	0.99
1613 + 658	8.89	-0.59	44.75	45.89 ± 0.11	0.4	0.4
1704 + 608	9.29	0.38	45.65	46.67 ± 0.21	0.1	0.1
2112 + 059	8.85	1.16	45.92	46.47 ± 0.02	-0.95	-1.0
2130 + 099	7.49	0.05	44.35	45.52 ± 0.32	0.95	0.99
2251 + 113	8.86	0.66	45.60	46.13 ± 0.01	-0.95	-1.0
2308 + 098	9.43	0.22	45.62	46.61 ± 0.22	0.4	0.5

Table 1: Spin parameters of quasars corresponding to  $r_2 = 0.1$  and  $r_2 = 0$  (for comparison with GR)

those spins are determined based on general relativity and are highly model dependent [82–84].

We note from Table 1 that nearly half of the quasars are maximally spinning with  $a \sim 0.95$  for  $r_2 \sim 0.1$  while  $a \sim 0.99$  when GR is assumed. By using the general relativistic disk reflection model [85], Crummy et al. [86] studied the spectra of several quasars reported in Table 1 (PG 0003+199, PG 0050+124, PG 1115+407, PG 1211+143, PG 1244+026, PG 1402+261, PG 1404+226, PG 1440+356) and arrived at a similar conclusion. In particular, the spin of PG 0003+199 (also known as Mrk335) is very well constrained, namely,  $a \sim 0.89 \pm 0.05$  [87] from its X-ray reflection spectrum and  $a \sim 0.83_{-0.13}^{+0.09}$  [80] from the relativistic broadening of the Fe- $K_\alpha$  line. These estimates are very much in agreement with our results based on general relativity, although their method of constraining the spin is different from ours. A study of the gravitationally red-shifted iron line of PG 1613+658 (Mrk 876) [88] reveals that the quasar harbors a rotating central black hole which is in agreement with our findings. From the polarimetric observations of AGNs, Afanasiev et al. [89] independently estimated the spins of some of the quasars reported in Table 1. Such an analysis corroborates our spin estimates for PG 0003+199, PG 0026+129, PG 0050+124, PG 0923+129, PG 0923+201, PG 2130+099 and PG 2308+098 although the results for PG 0921+525, PG 1022+519, PG 1425+267, PG 1545+210, PG 1613+658, PG 1704+608 shows some variations. However, the spin of PG 1704+608 (3C 351) estimated based on the correlation between the jet power with the black hole mass and spin [90] is consistent with our estimates of  $a \sim 0.1$ , assuming general relativity. Piotrovich et al. [65] constrained the spins of some of the radio-loud quasars [91, 92] in our sample, e.g. PG 1226+023 (3C 273), PG 1704+608 (3C 351) and PG 1100+772 to  $a < 1$ ,  $a < 0.998$  and  $a \sim 0.88_{-0.03}^{+0.02}$ , respectively. Our analysis reveals that PG 1704+608 and PG 1100+772 are slowly spinning prograde systems while PG 1226+023 harbors a maximally spinning retrograde black hole. Recent studies [93–96] show that retrograde black holes are associated with strong radio jets which is in accordance with the high radio luminosity observed in these systems [92, 97]. On the contrary, rapidly rotating prograde systems turn out to be radio-quiet, consistent with our findings [91, 98–100].

## 5 Summary and concluding remarks

In this work we attempt to discern the signatures of Einstein-Maxwell dilaton-axion (EMDA) gravity from the quasar continuum spectrum, which is believed to be an important astrophysical site to examine the nature of gravitational interaction in the high curvature regime. EMDA gravity arises in the low energy effective action of the heterotic string theory and bears the coupling of the scalar dilaton and the pseudo-scalar axion to the metric and the Maxwell field. The dilaton and the axion fields are inherited in the action from string compactifications and exhibit interesting implications in inflationary cosmology and the late time acceleration of the universe. Therefore, it is worthwhile to search for the imprints of these fields in the available astrophysical observations since this provides a testbed for string theory.

The presence of dilaton and axion in the theory results in substantial modifications of the gravitational field equations compared to general relativity. The stationary and axi-symmetric black hole solution of these equations leads to the Kerr-Sen metric which carries a dilaton charge with the axionic field imparting angular momentum to the black hole. The presence of the Maxwell field makes the Kerr-Sen black hole electrically charged and renders non-trivial field strengths to the axion and the dilaton. The electric charge of the black hole, however, stems from the axion-photon coupling and not the in-falling charged particles. In the absence of the Maxwell field the effect of dilaton and axion vanish and the Kerr-Sen metric reduces to the Kerr metric in general relativity.

The observational signatures of the Kerr-Sen spacetime has been explored in the context of strong

gravitational lensing and black hole shadows [39–42]. Therefore, in this work we investigate the impact of the dilaton-axion black holes on the quasar continuum spectrum which is believed to store a wealth of information regarding the background metric. Such an attempt has been recently made [101] although there, the authors have not compared the theoretical spectra with the observations. In this work we compute the theoretical estimate of optical luminosity for a sample of eighty Palomar Green quasars using the thin accretion disk model proposed by Novikov & Thorne. These are then compared with the corresponding optical observations of quasars to obtain an estimate of the observationally favored dilaton parameter and the angular momentum of the quasars. Our study brings out that  $0 \lesssim r_2 \lesssim 0.1$  is favored by the quasar optical data which is based on the analysis of the error estimators like the  $\chi^2$ , the Nash-Sutcliffe efficiency, the index of agreement and the modified versions of the last two.

The fact that  $r_2 \sim 0$  is supported by observations implies that the Kerr scenario is more favored compared to the Kerr-Sen background. This in turn indicates a negligible field strength for axion whose suppression has been observed in several other physical scenarios, e.g. in the inflationary era induced by higher curvature gravity [102, 103] and higher dimensions [104], in the warped braneworld scenario [105] with bulk Kalb-Ramond fields [106, 107] and the related stabilization of the modulus [108] and so on. We further point out that our results are in agreement with a previous work [77] where such a conclusion has been independently arrived by investigating the observed jet power and the radiative efficiencies of the microquasars with the corresponding theoretical estimates in the Kerr-Sen background. Also it is worthwhile to note that an observational verification of the Kerr solution ( $r_2 \sim 0$ ) does not confirm general relativity with certainty, since apart from general relativity, the Kerr metric represents the black hole solution for several other alternate gravity models [78].

The present analysis also allows us to constrain the spins of the quasars which are mostly in agreement with the previous estimates. However, there are limitations associated with spin measurements. This is because the spectral energy distribution (SED) of the quasars consists of emission from multiple components, e.g. the accretion disk, the corona, the jet and the dusty torus which are not always easy to observe and model [82]. Discerning the effect of each of these components from the SED is often very challenging which limits accurate determination of their mass, spin, distance and inclination. As a result the spin of the same quasar estimated by different methods often leads to inconsistent results [82–84, 109, 110].

We further note that the background metric affects the emission from only those components which reside close to the horizon. We are therefore interested in modelling the continuum spectrum from the accretion disk since its inner edge approaches the vicinity of the horizon. The continuum spectrum however, is not only sensitive to the background spacetime but also on the properties of the accretion flow. In the present work the spectrum is computed using the thin-disk approximation which does not take into account the presence of outflows or the radial velocity of the accretion flow. A more comprehensive modelling of the disk would therefore impose stronger constraints on the background metric. At present, these issues are addressed by considering several phenomenological models which is beyond the scope of this work.

Apart from the continuum spectrum, there exists other astrophysical observations e.g., the quasi-periodic oscillations observed in the power spectrum of black holes [111, 112], the broadened and skewed iron K- $\alpha$  line in the reflection spectrum of black holes [113, 114], and the black hole shadow [115–117], which can be used to further establish or falsify our present findings. We leave this study for a future work which will be reported elsewhere.

## 6 Acknowledgements

The research of SSG is partially supported by the Science and Engineering Research Board-Extra Mural Research Grant No. (EMR/2017/001372), Government of India.

## References

- [1] C. M. Will, “Was Einstein right?,” *Annalen Phys.* **15** (2005) 19–33, [arXiv:gr-qc/0504086 \[gr-qc\]](#). [Annalen Phys.518,19(2006)].
- [2] C. M. Will, *Theory and experiment in gravitational physics*. 1993.
- [3] C. M. Will, “The Confrontation between general relativity and experiment,” *Living Rev. Rel.* **9** (2006) 3, [arXiv:gr-qc/0510072 \[gr-qc\]](#).
- [4] E. Berti *et al.*, “Testing General Relativity with Present and Future Astrophysical Observations,” *Class. Quant. Grav.* **32** (2015) 243001, [arXiv:1501.07274 \[gr-qc\]](#).
- [5] **LIGO Scientific, VIRGO** Collaboration, B. P. Abbott *et al.*, “GW170104: Observation of a 50-Solar-Mass Binary Black Hole Coalescence at Redshift 0.2” *Phys. Rev. Lett.* **118** no. 22, (2017) 221101, [arXiv:1706.01812 \[gr-qc\]](#). [Erratum: Phys. Rev. Lett.121,no.12,129901(2018)].
- [6] **LIGO Scientific, Virgo** Collaboration, B. P. Abbott *et al.*, “Binary Black Hole Mergers in the first Advanced LIGO Observing Run,” *Phys. Rev.* **X6** no. 4, (2016) 041015, [arXiv:1606.04856 \[gr-qc\]](#). [erratum: Phys. Rev.X8,no.3,039903(2018)].
- [7] **LIGO Scientific, Virgo** Collaboration, B. P. Abbott *et al.*, “GW151226: Observation of Gravitational Waves from a 22-Solar-Mass Binary Black Hole Coalescence,” *Phys. Rev. Lett.* **116** no. 24, (2016) 241103, [arXiv:1606.04855 \[gr-qc\]](#).
- [8] **LIGO Scientific, Virgo** Collaboration, B. P. Abbott *et al.*, “Tests of general relativity with GW150914,” *Phys. Rev. Lett.* **116** no. 22, (2016) 221101, [arXiv:1602.03841 \[gr-qc\]](#). [Erratum: Phys. Rev. Lett.121,no.12,129902(2018)].
- [9] **LIGO Scientific, Virgo** Collaboration, B. P. Abbott *et al.*, “Observation of Gravitational Waves from a Binary Black Hole Merger,” *Phys. Rev. Lett.* **116** no. 6, (2016) 061102, [arXiv:1602.03837 \[gr-qc\]](#).
- [10] R. Penrose, “Gravitational collapse and space-time singularities,” *Phys. Rev. Lett.* **14** (1965) 57–59.
- [11] S. W. Hawking, “Breakdown of Predictability in Gravitational Collapse,” *Phys. Rev.* **D14** (1976) 2460–2473.
- [12] D. Christodoulou, “The formation of black holes and singularities in spherically symmetric gravitational collapse,” *Commun. Pure Appl. Math.* **44** no. 3, (1991) 339–373.
- [13] C. Rovelli, “Black hole entropy from loop quantum gravity,” *Phys. Rev. Lett.* **77** (1996) 3288–3291, [arXiv:gr-qc/9603063 \[gr-qc\]](#).

- [14] F. Dowker, “Causal sets and the deep structure of spacetime,” in *100 Years Of Relativity: space-time structure: Einstein and beyond*, A. Ashtekar, ed., pp. 445–464. 2005. [arXiv:gr-qc/0508109 \[gr-qc\]](#).
- [15] A. Ashtekar, T. Pawłowski, and P. Singh, “Quantum nature of the big bang,” *Phys. Rev. Lett.* **96** (2006) 141301, [arXiv:gr-qc/0602086 \[gr-qc\]](#).
- [16] J. Bekenstein and M. Milgrom, “Does the missing mass problem signal the breakdown of Newtonian gravity?,” *Astrophys. J.* **286** (1984) 7–14.
- [17] **Supernova Cosmology Project** Collaboration, S. Perlmutter *et al.*, “Measurements of Omega and Lambda from 42 high redshift supernovae,” *Astrophys. J.* **517** (1999) 565–586, [arXiv:astro-ph/9812133 \[astro-ph\]](#).
- [18] **Supernova Search Team** Collaboration, A. G. Riess *et al.*, “Observational evidence from supernovae for an accelerating universe and a cosmological constant,” *Astron. J.* **116** (1998) 1009–1038, [arXiv:astro-ph/9805201 \[astro-ph\]](#).
- [19] S. Nojiri and S. D. Odintsov, “Modified gravity with negative and positive powers of the curvature: Unification of the inflation and of the cosmic acceleration,” *Phys.Rev.* **D68** (2003) 123512, [arXiv:hep-th/0307288 \[hep-th\]](#).
- [20] S. Nojiri and S. D. Odintsov, “Modified f(R) gravity consistent with realistic cosmology: From matter dominated epoch to dark energy universe,” *Phys. Rev.* **D74** (2006) 086005, [arXiv:hep-th/0608008 \[hep-th\]](#).
- [21] S. Capozziello, S. Nojiri, S. D. Odintsov, and A. Troisi, “Cosmological viability of f(R)-gravity as an ideal fluid and its compatibility with a matter dominated phase,” *Phys. Lett.* **B639** (2006) 135–143, [arXiv:astro-ph/0604431 \[astro-ph\]](#).
- [22] C. Lanczos, “Electricity as a natural property of Riemannian geometry,” *Rev. Mod. Phys.* **39** (1932) 716–736.
- [23] C. Lanczos, “A Remarkable property of the Riemann-Christoffel tensor in four dimensions,” *Annals Math.* **39** (1938) 842–850.
- [24] D. Lovelock, “The Einstein tensor and its generalizations,” *J. Math. Phys.* **12** (1971) 498–501.
- [25] T. Padmanabhan and D. Kothawala, “Lanczos-Lovelock models of gravity,” *Phys. Rept.* **531** (2013) 115–171, [arXiv:1302.2151 \[gr-qc\]](#).
- [26] T. Shiromizu, K.-i. Maeda, and M. Sasaki, “The Einstein equation on the 3-brane world,” *Phys. Rev.* **D62** (2000) 024012, [arXiv:gr-qc/9910076 \[gr-qc\]](#).
- [27] N. Dadhich, R. Maartens, P. Papadopoulos, and V. Rezanian, “Black holes on the brane,” *Phys. Lett.* **B487** (2000) 1–6, [arXiv:hep-th/0003061 \[hep-th\]](#).
- [28] T. Harko and M. K. Mak, “Vacuum solutions of the gravitational field equations in the brane world model,” *Phys. Rev.* **D69** (2004) 064020, [arXiv:gr-qc/0401049 \[gr-qc\]](#).

- [29] T. R. P. Carames, M. E. X. Guimaraes, and J. M. Hoff da Silva, “Effective gravitational equations for  $f(R)$  braneworld models,” *Phys. Rev.* **D87** no. 10, (2013) 106011, [arXiv:1205.4980 \[gr-qc\]](#).
- [30] G. W. Horndeski, “Second-order scalar-tensor field equations in a four-dimensional space,” *Int. J. Theor. Phys.* **10** (1974) 363–384.
- [31] T. P. Sotiriou and S.-Y. Zhou, “Black hole hair in generalized scalar-tensor gravity,” *Phys. Rev. Lett.* **112** (2014) 251102, [arXiv:1312.3622 \[gr-qc\]](#).
- [32] E. Babichev, C. Charmousis, and A. Leibel, “Black holes and stars in Horndeski theory,” *Class. Quant. Grav.* **33** no. 15, (2016) 154002, [arXiv:1604.06402 \[gr-qc\]](#).
- [33] C. Charmousis and M. Tsoukalas, “Lovelock Galileons and black holes,” *Phys. Rev.* **D92** no. 10, (2015) 104050, [arXiv:1506.05014 \[gr-qc\]](#).
- [34] M. Cicoli and E. Di Valentino, “Fitting string inflation to real cosmological data,” [arXiv:2004.01210 \[astro-ph.CO\]](#).
- [35] A. Sen, “Rotating charged black hole solution in heterotic string theory,” *Phys. Rev. Lett.* **69** (1992) 1006–1009, [arXiv:hep-th/9204046](#).
- [36] M. Rogatko, “Positivity of energy in Einstein-Maxwell axion dilaton gravity,” *Class. Quant. Grav.* **19** (2002) 5063–5072, [arXiv:hep-th/0209126](#).
- [37] J. Sonner and P. K. Townsend, “Recurrent acceleration in dilaton-axion cosmology,” *Phys. Rev. D* **74** (2006) 103508, [arXiv:hep-th/0608068](#).
- [38] R. Catena and J. Moller, “Axion-dilaton cosmology and dark energy,” *JCAP* **03** (2008) 012, [arXiv:0709.1931 \[hep-ph\]](#).
- [39] G. N. Gylulchev and S. S. Yazadjiev, “Kerr-Sen dilaton-axion black hole lensing in the strong deflection limit,” *Phys. Rev. D* **75** (2007) 023006, [arXiv:gr-qc/0611110](#).
- [40] J. An, J. Peng, Y. Liu, and X.-H. Feng, “Kerr-Sen Black Hole as Accelerator for Spinning Particles,” *Phys. Rev. D* **97** no. 2, (2018) 024003, [arXiv:1710.08630 \[gr-qc\]](#).
- [41] Z. Younsi, A. Zhidenko, L. Rezzolla, R. Konoplya, and Y. Mizuno, “New method for shadow calculations: Application to parametrized axisymmetric black holes,” *Phys. Rev. D* **94** no. 8, (2016) 084025, [arXiv:1607.05767 \[gr-qc\]](#).
- [42] K. Hioki and U. Miyamoto, “Hidden symmetries, null geodesics, and photon capture in the Sen black hole,” *Phys. Rev. D* **78** (2008) 044007, [arXiv:0805.3146 \[gr-qc\]](#).
- [43] A. Narang, S. Mohanty, and A. Kumar, “Test of Kerr-Sen metric with black hole observations,” [arXiv:2002.12786 \[gr-qc\]](#).
- [44] G. Gibbons and K.-i. Maeda, “Black Holes and Membranes in Higher Dimensional Theories with Dilaton Fields,” *Nucl. Phys. B* **298** (1988) 741–775.
- [45] D. Garfinkle, G. T. Horowitz, and A. Strominger, “Charged black holes in string theory,” *Phys. Rev. D* **43** (1991) 3140. [Erratum: *Phys.Rev.D* 45, 3888 (1992)].

- [46] G. T. Horowitz and A. Strominger, “Black strings and P-branes,” *Nucl. Phys. B* **360** (1991) 197–209.
- [47] R. Kallosh and T. Ortin, “Charge quantization of axion - dilaton black holes,” *Phys. Rev. D* **48** (1993) 742–747, [arXiv:hep-th/9302109](#).
- [48] C. Ganguly and S. SenGupta, “Penrose process in a charged axion–dilaton coupled black hole,” *Eur. Phys. J. C* **76** no. 4, (2016) 213, [arXiv:1401.6826 \[hep-th\]](#).
- [49] A. Garcia, D. Galtsov, and O. Kechkin, “Class of stationary axisymmetric solutions of the Einstein-Maxwell dilaton - axion field equations,” *Phys. Rev. Lett.* **74** (1995) 1276–1279.
- [50] A. Ghezelbash and H. Siahhaan, “Hidden and Generalized Conformal Symmetry of Kerr-Sen Spacetimes,” *Class. Quant. Grav.* **30** (2013) 135005, [arXiv:1206.0714 \[hep-th\]](#).
- [51] C. Bernard, “Stationary charged scalar clouds around black holes in string theory,” *Phys. Rev. D* **94** no. 8, (2016) 085007, [arXiv:1608.05974 \[gr-qc\]](#).
- [52] S. Yazadjiev, “Exact static solutions in four-dimensional Einstein-Maxwell dilaton gravity,” *Int. J. Mod. Phys. D* **8** (1999) 635–643, [arXiv:gr-qc/9906048](#).
- [53] I. D. Novikov and K. S. Thorne, “Astrophysics of black holes.,” in *Black Holes (Les Astres Occlus)*, C. Dewitt and B. S. Dewitt, eds., pp. 343–450. 1973.
- [54] D. N. Page and K. S. Thorne, “Disk-Accretion onto a Black Hole. Time-Averaged Structure of Accretion Disk,” *Astrophys. J.* **191** (1974) 499–506.
- [55] I. Banerjee, S. Chakraborty, and S. SenGupta, “Decoding signatures of extra dimensions and estimating spin of quasars from the continuum spectrum,” [arXiv:1905.08043 \[gr-qc\]](#).
- [56] D. Ayzenberg and N. Yunes, “Black Hole Continuum Spectra as a Test of General Relativity: Quadratic Gravity,” *Class. Quant. Grav.* **34** no. 11, (2017) 115003, [arXiv:1701.07003 \[gr-qc\]](#).
- [57] J. Frank, A. King, and D. Raine, *Accretion Power in Astrophysics*. Cambridge University Press, Cambridge, UK, 2002.
- [58] M. Schmidt and R. F. Green, “Quasar evolution derived from the Palomar bright quasar survey and other complete quasar surveys,” *Astrophys. J.* **269** (1983) 352.
- [59] S. W. Davis and A. Laor, “The Radiative Efficiency of Accretion Flows in Individual AGN,” *Astrophys. J.* **728** (2011) 98, [arXiv:1012.3213 \[astro-ph.CO\]](#).
- [60] S. Kaspi, P. S. Smith, H. Netzer, D. Maoz, B. T. Jannuzi, and U. Giveon, “Reverberation measurements for 17 quasars and the size mass luminosity relations in active galactic nuclei,” *Astrophys. J.* **533** (2000) 631, [arXiv:astro-ph/9911476 \[astro-ph\]](#).
- [61] S. Kaspi, D. Maoz, H. Netzer, B. M. Peterson, M. Vestergaard, and B. T. Jannuzi, “The Relationship between luminosity and broad-line region size in active galactic nuclei,” *Astrophys. J.* **629** (2005) 61–71, [arXiv:astro-ph/0504484 \[astro-ph\]](#).
- [62] T. A. Boroson and R. F. Green, “The Emission - line properties of low - redshift quasi-stellar objects,” *Astrophys. J. Suppl.* **80** (1992) 109.

- [63] B. M. Peterson *et al.*, “Central masses and broad-line region sizes of active galactic nuclei. II. A Homogeneous analysis of a large reverberation-mapping database,” *Astrophys. J.* **613** (2004) 682–699, [arXiv:astro-ph/0407299](#) [astro-ph].
- [64] S. Wu, Y. Lu, F. Zhang, and Y. Lu, “Radiative Efficiency of Disk Accretion in Individual SDSS QSOs,” *Mon. Not. Roy. Astron. Soc.* **436** (2013) 3271, [arXiv:1310.0560](#) [astro-ph.CO].
- [65] M. Y. Piotrovich, Y. N. Gnedin, T. M. Natsvlshvili, and S. D. Buliga, “Constraints on spin of a supermassive black hole in quasars with big blue bump,” *ApSS* **362** (Dec., 2017) 231, [arXiv:1711.07272](#).
- [66] G. Neugebauer, R. F. Green, K. Matthews, M. Schmidt, B. T. Soifer, and J. Bennett, “Continuum energy distributions of quasars in the Palomar-Green Survey,” *Astrophys. J.* **63** .
- [67] A. Baskin and A. Laor, “What controls the C IV line profile in active galactic nuclei?,” *Mon. Not. Roy. Astron. Soc.* **356** (2005) 1029–1044, [arXiv:astro-ph/0409196](#) [astro-ph].
- [68] J. E. Scott, G. A. Kriss, M. Brotherton, R. F. Green, J. Hutchings, J. M. Shull, and W. Zheng, “A Composite extreme ultraviolet QSO spectrum from FUSE,” *Astrophys. J.* **615** (2004) 135–149, [arXiv:astro-ph/0407203](#) [astro-ph].
- [69] W. N. Brandt, A. Laor, and B. J. Wills, “On the Nature of soft x-ray weak quasistellar objects,” *Astrophys. J.* **528** (2000) 637–649, [arXiv:astro-ph/9908016](#) [astro-ph].
- [70] R. Andrae, T. Schulze-Hartung, and P. Melchior, “Dos and don’ts of reduced chi-squared,” [arXiv:1012.3754](#) [astro-ph.IM].
- [71] J. Nash and J. Sutcliffe, “River flow forecasting through conceptual models part i a discussion of principles,” *Journal of Hydrology* **10** no. 3, (1970) 282 – 290. <http://www.sciencedirect.com/science/article/pii/0022169470902556>.
- [72] D. R. Legates and G. J. McCabe, “Evaluating the use of goodness-of-fit measures in hydrologic and hydroclimatic model validation,” *Water Resources Research* **35** no. 1, (1999) 233–241. <http://dx.doi.org/10.1029/1998WR900018>.
- [73] P. Krause, D. P. Boyle, and F. Bäse, “Comparison of different efficiency criteria for hydrological model assessment,” *Advances in Geosciences* **5** (Dec., 2005) 89–97.
- [74] M. Goyal and B. Panigrahi, “Modeling methods and practices in soil and water engineering,” *New York: Apple Academic Press* (May, 2016) .
- [75] C. J. Willmott, “On the evaluation of model performance in physical geography,” in *Spatial statistics and models*, pp. 443–460. Springer, 1984.
- [76] C. J. Willmott, “On the validation of models,” *Physical Geography* **2** no. 2, (1981) 184–194, <http://www.tandfonline.com/doi/pdf/10.1080/02723646.1981.10642213>, <http://www.tandfonline.com/doi/abs/10.1080/02723646.1981.10642213>.
- [77] I. Banerjee, B. Mandal, and S. SenGupta, “Signatures of Einstein-Maxwell dilaton-axion gravity from the observed jet power and the radiative efficiency,” [arXiv:2007.03947](#) [gr-qc].

- [78] D. Psaltis, D. Perrodin, K. R. Dienes, and I. Mocioiu, “Kerr Black Holes are Not Unique to General Relativity,” *Phys. Rev. Lett.* **100** (2008) 091101, [arXiv:0710.4564 \[astro-ph\]](#).
- [79] I. Banerjee, S. Chakraborty, and S. SenGupta, “Excavating black hole continuum spectrum: Possible signatures of scalar hairs and of higher dimensions,” *Phys. Rev.* **D96** no. 8, (2017) 084035, [arXiv:1707.04494 \[gr-qc\]](#).
- [80] D. J. Walton, E. Nardini, A. C. Fabian, L. C. Gallo, and R. C. Reis, “Suzaku observations of ‘bare’ active galactic nuclei,” *Mon. Not. Roy. Astron. Soc.* **428** (2013) 2901, [arXiv:1210.4593 \[astro-ph.HE\]](#).
- [81] C. Bambi and E. Barausse, “Constraining the quadrupole moment of stellar-mass black-hole candidates with the continuum fitting method,” *Astrophys. J.* **731** (2011) 121, [arXiv:1012.2007 \[gr-qc\]](#).
- [82] L. Brenneman, “Measuring Supermassive Black Hole Spins in Active Galactic Nuclei,” [arXiv:1309.6334 \[astro-ph.HE\]](#).
- [83] C. S. Reynolds, “Measuring Black Hole Spin using X-ray Reflection Spectroscopy,” *Space Sci. Rev.* **183** no. 1-4, (2014) 277–294, [arXiv:1302.3260 \[astro-ph.HE\]](#).
- [84] C. S. Reynolds, “Observing black holes spin,” *Nat. Astron.* **3** no. 1, (2019) 41–47.
- [85] R. R. Ross and A. C. Fabian, “A Comprehensive range of x-ray ionized reflection models,” *Mon. Not. Roy. Astron. Soc.* **358** (2005) 211–216, [arXiv:astro-ph/0501116 \[astro-ph\]](#).
- [86] J. Crummy, A. C. Fabian, L. Gallo, and R. Ross, “An explanation for the soft x-ray excess in agn,” *Mon. Not. Roy. Astron. Soc.* **365** (2006) 1067–1081, [arXiv:astro-ph/0511457 \[astro-ph\]](#).
- [87] L. Keek and D. R. Ballantyne, “Revealing the accretion disc corona in Mrk 335 with multi-epoch X-ray spectroscopy,” *Mon. Not. Roy. Astron. Soc.* **456** no. 3, (2016) 2722–2734, [arXiv:1508.06994 \[astro-ph.HE\]](#).
- [88] E. Bottacini, E. Orlando, J. Greiner, M. Ajello, I. Moskalenko, and M. Persic, “An extreme gravitationally redshifted iron line at 4.8 keV in Mrk 876,” *Astrophys. J.* **798** (2015) L14, [arXiv:1412.3112 \[astro-ph.HE\]](#).
- [89] V. L. Afanasiev, Yu. N. Gnedin, M. Yu. Piotrovich, S. D. Buliga, and T. M. Natsvlshvili, “Determination of Supermassive Black Hole Spins Based on the Standard ShakuraSunyaev Accretion Disk Model and Polarimetric Observations,” *Astron. Lett.* **44** no. 6, (2018) 362–369.
- [90] R. A. Daly and T. B. Sprinkle, “Black Hole Spin Properties of 130 AGN,” *Mon. Not. Roy. Astron. Soc.* **438** no. 4, (2014) 3233–3242, [arXiv:1312.4862 \[astro-ph.CO\]](#).
- [91] M. Sikora, L. Stawarz, and J.-P. Lasota, “Radio-loudness of active galactic nuclei: observational facts and theoretical implications,” *Astrophys. J.* **658** (2007) 815–828, [arXiv:astro-ph/0604095 \[astro-ph\]](#).
- [92] R. V. Vasudevan and A. C. Fabian, “Piecing Together the X-ray Background: Bolometric Corrections for Active Galactic Nuclei,” *Mon. Not. Roy. Astron. Soc.* **381** (2007) 1235, [arXiv:0708.4308 \[astro-ph\]](#).

- [93] C. S. Reynolds, D. Garofalo, and M. C. Begelman, “Trapping of magnetic flux by the plunge region of a black hole accretion disk,” *Astrophys. J.* **651** (2006) 1023–1030, [arXiv:astro-ph/0607381](#) [[astro-ph](#)].
- [94] D. Garofalo, D. A. Evans, and R. M. Sambruna, “The Evolution of Radio Loud Active Galactic Nuclei as a Function of Black Hole Spin,” *Mon. Not. Roy. Astron. Soc.* **406** (2010) 975–986, [arXiv:1004.1166](#) [[astro-ph.CO](#)].
- [95] D. Garofalo, “The spin dependence of the Blandford-Znajek effect,” *Astrophys. J.* **699** (2009) 400–408, [arXiv:0904.3486](#) [[astro-ph.HE](#)].
- [96] D. Garofalo, “Retrograde versus prograde models of accreting black holes,” *Adv. Astron.* **2013** (2013) 213105, [arXiv:1304.3397](#) [[astro-ph.HE](#)].
- [97] M. Polletta, T. J. L. Courvoisier, E. J. Hooper, and B. J. Wilkes, “The far-infrared emission of radio loud and radio quiet quasars,” *Astron. Astrophys.* **362** (2000) 75, [arXiv:astro-ph/0006315](#) [[astro-ph](#)].
- [98] K. I. Kellermann, R. Sramek, M. Schmidt, D. B. Shaffer, and R. Green, “VLA observations of objects in the Palomar Bright Quasar Survey,” *Astron. J.* **98** (1989) 1195–1207.
- [99] R. Barvainis, J. Lehar, M. Birkinshaw, H. Falke, and K. M. Blundell, “Radio variability of radio quiet and radio loud quasars,” *Astrophys. J.* **618** (2004) 108–122, [arXiv:astro-ph/0409554](#) [[astro-ph](#)].
- [100] C. Villforth, K. Nilsson, R. Ostensen, J. Heidt, S. M. Niemi, and J. Pforr, “Intranight polarization variability in radio-loud and radio-quiet AGN,” *Mon. Not. Roy. Astron. Soc.* **397** (2009) 1893, [arXiv:0904.1598](#) [[astro-ph.CO](#)].
- [101] M. Heydari-Fard, M. Heydari-Fard, and H. R. Sepangi, “Thin accretion disks and charged rotating dilaton black holes,” *Eur. Phys. J. C* **80** no. 4, (2020) 351, [arXiv:2004.05552](#) [[gr-qc](#)].
- [102] E. Elizalde, S. D. Odintsov, T. Paul, and D. Sez-Chilln Gmez, “Inflationary universe in  $F(R)$  gravity with antisymmetric tensor fields and their suppression during its evolution,” *Phys. Rev. D* **99** no. 6, (2019) 063506, [arXiv:1811.02960](#) [[gr-qc](#)].
- [103] E. Elizalde, S. D. Odintsov, V. K. Oikonomou, and T. Paul, “Logarithmic-corrected  $R^2$  Gravity Inflation in the Presence of Kalb-Ramond Fields,” *JCAP* **1902** (2019) 017, [arXiv:1810.07711](#) [[gr-qc](#)].
- [104] T. Paul and S. SenGupta, “Dynamical suppression of spacetime torsion,” *Eur. Phys. J. C* **79** no. 7, (2019) 591, [arXiv:1808.00172](#) [[gr-qc](#)].
- [105] L. Randall and R. Sundrum, “A Large mass hierarchy from a small extra dimension,” *Phys. Rev. Lett.* **83** (1999) 3370–3373, [arXiv:hep-ph/9905221](#) [[hep-ph](#)].
- [106] B. Mukhopadhyaya, S. Sen, and S. SenGupta, “Bulk torsion fields in theories with large extra dimensions,” *Phys. Rev. D* **65** (2002) 124021, [arXiv:hep-ph/0110308](#) [[hep-ph](#)].

- [107] B. Mukhopadhyaya, S. Sen, and S. SenGupta, “Does a Randall-Sundrum scenario create the illusion of a torsion free universe?,” *Phys. Rev. Lett.* **89** (2002) 121101, [arXiv:hep-th/0204242 \[hep-th\]](#). [Erratum: *Phys. Rev. Lett.* 89,259902(2002)].
- [108] A. Das, B. Mukhopadhyaya, and S. SenGupta, “Why has spacetime torsion such negligible effect on the Universe?,” *Phys. Rev.* **D90** no. 10, (2014) 107901, [arXiv:1410.0814 \[hep-th\]](#).
- [109] J. F. Steiner, R. C. Reis, A. C. Fabian, R. A. Remillard, J. E. McClintock, L. Gou, R. Cooke, L. W. Brenneman, and J. S. Sanders, “A Broad Iron Line in LMC X-1,” *Mon. Not. Roy. Astron. Soc.* **427** (2012) 2552, [arXiv:1209.3269 \[astro-ph.HE\]](#).
- [110] L. Gou, J. E. McClintock, J. Liu, R. Narayan, J. F. Steiner, R. A. Remillard, J. A. Orosz, and S. W. Davis, “A Determination of the Spin of the Black Hole Primary in LMC X-1,” *Astrophys. J.* **701** (2009) 1076–1090, [arXiv:0901.0920 \[astro-ph.HE\]](#).
- [111] A. Maselli, L. Gualtieri, P. Pani, L. Stella, and V. Ferrari, “Testing Gravity with Quasi Periodic Oscillations from accreting Black Holes: the Case of the Einstein-Dilaton-Gauss-Bonnet Theory,” *Astrophys. J.* **801** no. 2, (2015) 115, [arXiv:1412.3473 \[astro-ph.HE\]](#).
- [112] G. Pappas, “What can quasi-periodic oscillations tell us about the structure of the corresponding compact objects?,” *Mon. Not. Roy. Astron. Soc.* **422** (2012) 2581–2589, [arXiv:1201.6071 \[astro-ph.HE\]](#).
- [113] C. Bambi, A. Cardenas-Avendano, T. Dauser, J. A. Garcia, and S. Nampalliwar, “Testing the Kerr black hole hypothesis using X-ray reflection spectroscopy,” *Astrophys. J.* **842** no. 2, (2017) 76, [arXiv:1607.00596 \[gr-qc\]](#).
- [114] Y. Ni, J. Jiang, and C. Bambi, “Testing the Kerr metric with the iron line and the KRZ parametrization,” *JCAP* **1609** no. 09, (2016) 014, [arXiv:1607.04893 \[gr-qc\]](#).
- [115] **Event Horizon Telescope** Collaboration, K. Akiyama *et al.*, “First M87 Event Horizon Telescope Results. II. Array and Instrumentation,” *Astrophys. J.* **875** no. 1, (2019) L2, [arXiv:1906.11239 \[astro-ph.IM\]](#).
- [116] **Event Horizon Telescope** Collaboration, K. Akiyama *et al.*, “First M87 Event Horizon Telescope Results. V. Physical Origin of the Asymmetric Ring,” *Astrophys. J.* **875** no. 1, (2019) L5, [arXiv:1906.11242 \[astro-ph.GA\]](#).
- [117] **Event Horizon Telescope** Collaboration, K. Akiyama *et al.*, “First M87 Event Horizon Telescope Results. VI. The Shadow and Mass of the Central Black Hole,” *Astrophys. J.* **875** no. 1, (2019) L6.